Coherent spinor dynamics in a spin-1 Bose condensate

MING-SHIEN CHANG, QISHU QIN, WENXIAN ZHANG, LI YOU AND MICHAEL S. CHAPMAN*

School of Physics, Georgia Institute of Technology, Atlanta, Georgia 30332-0430, USA

*e-mail: michael.chapman@physics.gatech.edu

Published online: 30 October 2005; doi:10.1038/nphys153

Collisions in a thermal gas are perceived as random or incoherent as a consequence of the large numbers of initial and final quantum states accessible to the system. In a quantum gas, for example, a Bose–Einstein condensate or a degenerate Fermi gas, the phase space accessible to low-energy collisions is so restricted that collisions become coherent and reversible. Here, we report the observation of coherent spin-changing collisions in a gas of spin-1 bosons. Starting with condensates occupying two spin states, a condensate in the third spin state is coherently and reversibly created by atomic collisions. The observed dynamics are analogous to Josephson oscillations in weakly connected superconductors and represent a type of matter–wave four-wave mixing. The spin-dependent scattering length is determined from these oscillations to be $-1.45(32)$ bohr. Finally, we demonstrate coherent control of the evolution of the system by applying differential phase shifts to the spin states using magnetic fields.

Bose–Einstein condensation is a well-known phenomenon in which identical bosons occupy the same quantum state below a certain critical temperature. A hallmark of Bose–Einstein condensation is the coherence between particles—every particle shares the same quantum wavefunction and phase. Although textbook discussions of Bose–Einstein condensation typically focus on non-interacting (ideal) particles, elastic collisions are essential in order for a quantum degenerate gas to equilibrate. The inclusion of collisions also modifies the quantum ground state of the gas, although it does not change the nature of the coherence of the condensate—indeed it has been pointed out that collisional interactions are in fact required to keep the condensate from fragmenting into multiple nearby quantum states[1].

Collisional coherence is an important theme in quantum degenerate gases. For single-component condensates, such as spin-polarized atomic condensates confined in a magnetic trap, the coherence of the collisional interactions has been well demonstrated in early measurements of condensate mean-field energy[2] and correlations[3], as well as in demonstrations of matter–wave interference[4] and superfluid behaviour[5–7]. Collisional coherence in more complicated systems has led to remarkable demonstrations, including reversible atom–molecule formation across a Feshbach resonance for both bosonic and fermionic[8,9] atoms, and coherent collisions in optical lattices[10,11].

In this work, we show that the collisional coherence extends to the internal spin degrees of freedom of a spin-1 Bose gas by observing coherent and reversible spin-changing collisions. Atomic Bose condensates with internal spin, so-called spinor condensates[12–20], in some cases are predicted to coherently interconvert in a process known as spin mixing, driven solely by internal interactions in the system[21–26]. In a spin-1 condensate, two atoms with spin components -1 and $+1$ can coherently and reversibly scatter into final states containing two atoms with spin component 0, and *vice versa* (Fig. 1a). We observe this process in a gas of spin-1 ^{87}Rb bosons confined in an all-optical trap. The coherent spin mixing leads to oscillations of the spin populations, from which we determine the spin-dependent interaction strength. This is the first direct measurement of this important quantity. The observed spin mixing is an internal-state analogue to Josephson oscillations in weakly connected superconductors[27], and, exploiting this analogy, we demonstrate control of the coherent spinor dynamics using

phase and population engineering. Finally, we use this technique to drive the spinor condensate to and away from its spin ground state, which allows us to measure the spin-coherence time[21].

Stimulated by the seminal theoretical works of Ho[12] and Ohmi and Machida[13] and early experiments by the JILA[14,28] and MIT[15] groups, much study has been done on spinor condensates. Theoretical work has covered ground-state structure[12,13,20,21,29], coherent spinor dynamics[21–26], rotating spinor condensates[30] and many other topics. Spin mixing has been observed in both spin $F=1$ and $F=2$ condensates[15,18,19,31], although the coherence of this process has not yet been demonstrated conclusively. Observations thus far have revealed mostly incoherent relaxation of initially non-equilibrium spin populations to lower energy configurations from which the sign of the spin interaction parameter c_2 was determined. Although overdamped single oscillations in spin populations have been observed in experiments by us and others, their interpretation has been limited because the initial spin configurations in these experiments were metastable, and evolution from these states is noise driven[15,18,19,31]. Nonetheless, from these observations, as well as studies of spin domain formation, it was possible to determine the magnetic nature of the ground states.

At the microscopic level, the interactions in spinor Bose gases are determined by spin-dependent two-body collisions. In the case of two colliding spin-F identical bosons, the available collision channels are restricted by symmetry to those with total spin $F_{\rm tot}=2F,2F-2,\ldots,0$ characterized by s-wave scattering lengths $a_{F_{\rm tot}}$ at low energies. We focus on the $F=1$ case here, and, in the framework of mean-field theory, the interaction energy including spin can be written as $U(r)=\delta(r)(c_0+c_2\mathbf{F}_a\cdot\mathbf{F}_b)$, refs 12,13, where $\delta(r)$ is the Dirac delta function, r is the distance between two atoms a,b and $c_0=4\pi\hbar^2(a_0+2a_2)/3m$ and $c_2=4\pi\hbar^2(a_2-a_0)/3m$, where $\hbar$ is the reduced Planck constant, m is the atomic mass and $a_{0,2}$ are the s-wave scattering lengths for the total spin-0, 2 channels. For ^{87}Rb atoms in the $F=1$ hyperfine state, the scattering lengths $a_{0,2}$ are nearly equal, and hence the spin-dependent mean-field energy c_2n is very small (only 200 pK, refs 32,33, for typical densities $n\sim10^{14}$ cm^{-3}) compared with both the scalar mean field, c_0n, and the estimated temperature of the gas, ~50 nK. Nonetheless, the small spin-dependent mean-field couplings are non-negligible and lead to qualitatively different ground-state structures depending on the sign of c_2, being ferromagnetic ($c_2<0$) for ^{87}Rb (refs 18, 19,32,33) or anti-ferromagnetic ($c_2>0$) for ^{23}Na (refs 15,34). Moreover, these spinor interactions yield a rich variety of coherent and incoherent phenomena including coherent spinor mixing, spin squeezing and entanglement[21,35], spin domain formation and spinor vortices.

A single-component (scalar) atomic condensate with a large number of atoms is well described within a mean-field treatment by an order parameter (condensate wavefunction) governed by the nonlinear Schrödinger or Gross–Pitaevskii equation. For an $F=1$ spinor condensate, the three Zeeman components with magnetic quantum numbers $m_F=1,0,-1$ are described by a vector order parameter $\boldsymbol{\psi}(\mathbf{r},t)=(\psi_1,\psi_0,\psi_{-1})$, which is governed by a set of three coupled Gross–Pitaevskii equations[12,21]:

$$i\hbar\frac{\partial\psi_1}{\partial t}=L_1\psi_1+c_2(n_1+n_0-n_{-1})\psi_1+c_2\psi_0^2\psi_{-1}^*, \quad (1)$$

$$i\hbar\frac{\partial\psi_0}{\partial t}=L_0\psi_0+c_2(n_1+n_{-1})\psi_0+2c_2\psi_0^*\psi_1\psi_{-1}, \quad (2)$$

$$i\hbar\frac{\partial\psi_{-1}}{\partial t}=L_{-1}\psi_{-1}+c_2(n_{-1}+n_0-n_1)\psi_{-1}+c_2\psi_0^2\psi_{+1}^*, \quad (3)$$

where $L_{\pm1,0}=(-\hbar^2\nabla^2/2m+V_{\rm t}+E_{\pm1,0}+c_0n-\mu)$, $V_{\rm t}$, $E_{\pm1,0}$ and $n_{\pm1,0}$ are the optical trapping potential, Zeeman energies and densities for the corresponding Zeeman projections, μ is the chemical

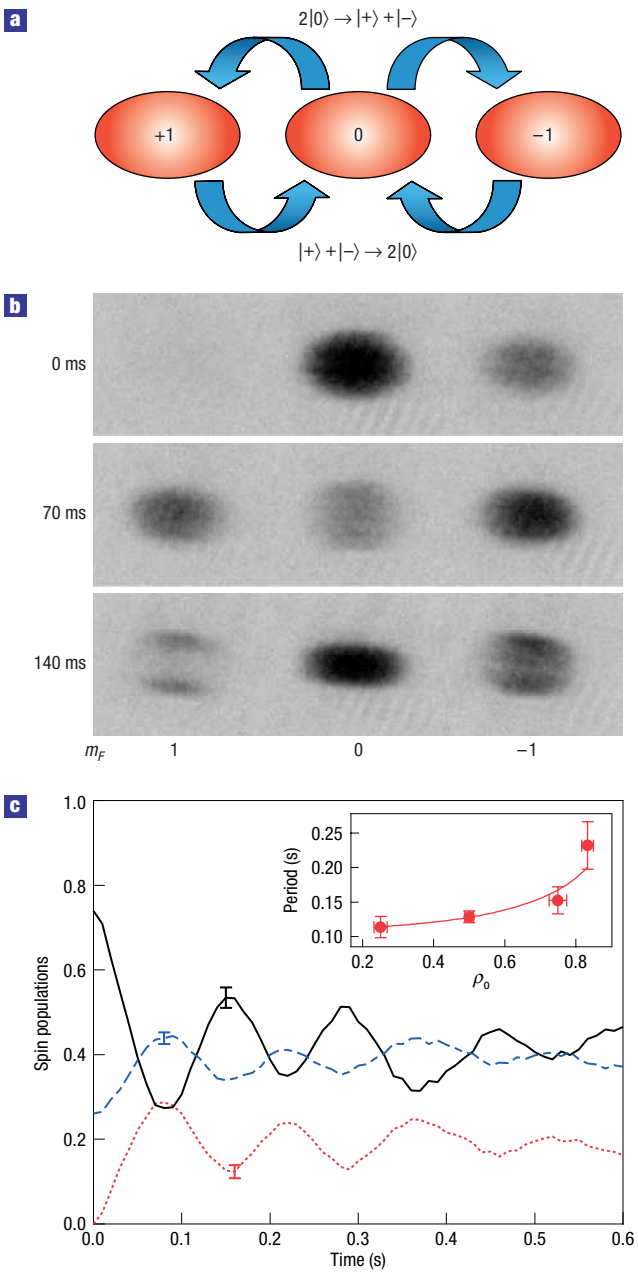

Figure 1 Coherent spin mixing of spin-1 Bose condensate in an optical trap. The $F=1$, $m_F=1,0,-1$ spin states of ^{87}Rb condensates confined in an optical trap start from a superposition of spin components at $t=0$. They are allowed to evolve freely to initiate coherent spin mixing, which results in oscillations of their populations. **a**, The schematic indicates the fundamental spin-mixing process. **b**, Absorptive images of the condensates for different evolution times. In this example, the initial relative populations are $\rho_{(1,0,-1)}\simeq(0,3/4,1/4)$. The condensates are probed 18 ms after release from the trap and, to separate the spin components for imaging, a weak magnetic field gradient is applied for 3 ms during expansion of the condensates. The field of view is 600 μm × 180 μm. **c**, Spin populations versus evolution time for the same initial population configuration showing four clear oscillations. The damping of the oscillations is due to the breakdown of the SMA readily apparent in the $t=140$ ms absorptive image. Here the dotted, solid and dashed lines represent the populations in the $m_F=1,0$ and -1 states, respectively. The inset shows the measured oscillation period versus the initial population of the 0 state for different initial superpositions of $m_F=0,-1$ states, which compares well with the theoretical prediction[23]. The (typical) error bars shown are the standard deviation of three repeated measurements.

potential, $n = n_1 + n_0 + n_{-1}$ is the total density. The coherent spin mixings of the internal populations responsible for oscillations of the spin populations are determined by the last terms in equations (1)–(3). However, the interplay of this process with the particle exchange collisions, represented by the penultimate terms in equations (1)–(3), poses challenging problems both in theory and in experiment. This is because both types of spinor dynamics occur with the same timescale (typically <10 Hz for ^{87}Rb) and they are both very sensitive to the external magnetic fields and field gradients represented in $E_{\pm1,0}$ (refs 15,18,20,26,31,36,37). Hence, in general, the dynamics described by these equations reveal a rich coupling between the internal and external degrees of freedom of the condensate components resulting in a variety of observed phenomena, including spin mixing[15,18,19], spin domain formation[15] and spin textures[30,38].

Although the internal and external dynamics are generally non-separable, under certain conditions they can be decoupled. In particular, when the available spin interaction energy is insufficient to create spatial spin structures in the condensates, then the external dynamics will be suppressed. This occurs when the spin healing length $\xi_s = 2\pi\hbar/\sqrt{2m|c_2|n}$ is larger than the size of the condensate. In this case, ψ_1, ψ_0 and ψ_{-1} share the same spatial wavefunction $\sqrt{n(\mathbf{r})}e^{-i\mu t/\hbar}$, which allows for a considerable simplification of equations (1)–(3). This is known as the single-mode approximation (SMA), with which the order parameter reduces to $\sqrt{n(\mathbf{r})}e^{-i\mu t/\hbar}\boldsymbol{\chi}$, where $\boldsymbol{\chi}^{\mathrm{T}} = (\sqrt{\rho_1}e^{i\phi_1}, \sqrt{\rho_0}e^{i\phi_0}, \sqrt{\rho_{-1}}e^{i\phi_{-1}})$ and ρ_i and ϕ_i represent the fractional population and phase of the ith Zeeman state. With this approximation, the internal dynamics take on a particularly simple form determined by just two dynamical variables: $\rho_0(t)$, the fractional population of the 0 state, and $\phi(t) \equiv \phi_+ + \phi_- - 2\phi_0$, the relative phase of the spinor components[23]. The populations of the other states are directly determined by $\rho_{\pm1} = (1 - \rho_0 \pm M)/2$, where $M = (N_{+1} - N_{-1})/N$ is the global magnetism, which is a constant of the motion, and N_i is the number of atoms in the ith Zeeman projection with $N = N_{-1} + N_0 + N_1$. The internal energy (hamiltonian) of the system in a uniform magnetic field then takes the following simple form[25,26]:

$$E = c\rho_0[(1 - \rho_0 + \sqrt{(1-\rho_0)^2 - M^2}\cos\phi)] + \delta(1 - \rho_0), \qquad (4)$$

where $c = c_2 N \int |\psi(r)|^4 \mathrm{d}r$ is the effective spin-mixing rate, and $\delta = (E_{+1} + E_{-1} - 2E_0)/2 \simeq 2\pi\hbar \cdot (72B^2$ Hz) is the difference in energies of the magnetic Zeeman levels in a field of B gauss. Within the SMA, the ground-state spin populations and relative phase are readily found for arbitrary magnetization and magnetic field by minimizing equation (4). In particular, for $c(c_2) < 0$, the energy of the system is minimized at low fields for relative phases $\phi = 0$ and population $\rho_0 = (1 - M^2)/2$ (refs 23,26). For other non-equilibrium populations or phases, the system will have excess spin energy that can drive a coherent evolution of the spinor system.

The evolution of the system will follow hamiltonian equations of motion derived from equation (4), ref. 26:

$$\dot{\rho}_0 = \frac{2c}{\hbar}\rho_0\sqrt{(1-\rho_0)^2 - M^2}\sin\phi, \qquad (5)$$

$$\dot{\phi} = -\frac{2\delta}{\hbar} + \frac{2c}{\hbar}(1 - 2\rho_0) + \frac{2c}{\hbar}\frac{(1-\rho_0)(1-2\rho_0) - M^2}{\sqrt{(1-\rho_0)^2 - M^2}}\cos\phi. \qquad (6)$$

These coupled equations are nonlinear Josephson-type equations and point to the equivalency of spin mixing in a spin-1 condensate to Josephson systems realized in superconductors[27] and other superfluids[11,14,39–44]. The nonlinearity of these equations provides a rich manifold of dynamical trajectories that can be accessed experimentally by choice of initial populations and phases of the spin components and the strength of the applied magnetic field.

To investigate the coherent dynamics of this system, we begin with ^{87}Rb condensates created using an improved version of the all-optical trapping technique we have previously reported[16,19]. Using a dynamical compression technique and just a single focused laser beam[45], condensates with up to 300,000 atoms are created after 2 s of evaporative cooling. The condensates created in this optical trap are generally in a mixture of all $F = 1$ spin states and reveal complicated spatial domains. To create a well-characterized initial condition, we first prepare a condensate in the $|F = 1, m_F = -1\rangle$ state by applying a magnetic field gradient during the evaporative cooling.

To initiate spin dynamics, a coherent superposition of spin states with non-equilibrium spin populations is created by applying a sequence of phase-coherent microwave pulses tuned to the $F = 1 \leftrightarrow F = 2$ transitions. Following this state preparation, the condensate is allowed to evolve freely in the optical trap. A typical evolution is shown in Fig. 1c for an initial spin configuration of $\rho_{(1,0,-1)} \simeq (0, 3/4, 1/4)$. Up to four distinct oscillations are observed in this example before the spin populations damp to a steady state. These oscillations demonstrate the coherence of the spin-mixing process.

We have measured the spin oscillation frequency for different initial spin populations. These data are shown in the inset of Fig. 1c and show good agreement with theoretical predictions where $c\sqrt{1-\rho_0^2}$ (refs 23,26), which can be derived from equations (5) and (6). These measurements provide a direct determination of the magnitude of the spin interaction energy[21], $|c|/\hbar = 2\pi \times 4.3(3)$ rad s^{-1} for our system. These oscillation frequencies at low magnetic field do not determine the sign of $c(c_2)$; however, it was established by previous studies of the nature of the ground state (and confirmed in the present study by the results shown later in Fig. 3) that $c_2 < 0$ for the $F = 1$ manifold of ^{87}Rb. This value of c, combined with the measured condensate density $n = 2.1(4) \times 10^{14}$ cm^{-3}, determined from the rate of the condensate expansion during time-of-flight, permits determination of c_2 or, equivalently, the difference in scattering lengths $a_2 - a_0 = -1.45(32)a_B$, where the Bohr radius $a_B = 0.529$ Å. This is the first direct measurement of this important quantity, and our value agrees with the theoretical determination of $a_2 - a_0 = -1.40(22)a_B$ derived from photo-associative spectroscopy and Feshbach resonance data[32,33].

The oscillations are observed to damp with a time constant of 250 ms, and the damping coincides with the appearance of spatial spin structures apparent in the images in Fig. 1b. These structures indicate the invalidation of the SMA underlying equations (5) and (6) and lead to a complicated interplay of the internal and external dynamics that ultimately transfers the internal spin energy into spatial domain structures[23]. A detailed study of these structures will be the focus of future work.

The large-amplitude oscillations observed in Fig. 1c are in the nonlinear regime of equations (5) and (6). It is also possible to access the linear regime more typical of the standard Josephson effect by tuning the parameters of the system. In particular, for large applied magnetic fields such that $\delta \gg c$ and appropriate initial populations, the phase evolution is dominated by the quadratic Zeeman effect of the external field, and equation (6) reduces to $\dot{\phi} \cong -2\delta/\hbar$. For these conditions, the system shows small oscillations analogous to a.c. Josephson oscillations, $\rho_0(t) \simeq A\delta^{-1}\sin 2\delta t$, where A is determined by the initial populations. We have observed these oscillations as shown in Fig. 2 for different applied magnetic fields. Up to 12 fast oscillations are observed at the highest fields that were studied, where the timescale of the internal spinor dynamics is much shorter than the timescale for the formation of the spatial spin structures. The frequency of the measured oscillations versus the magnetic field

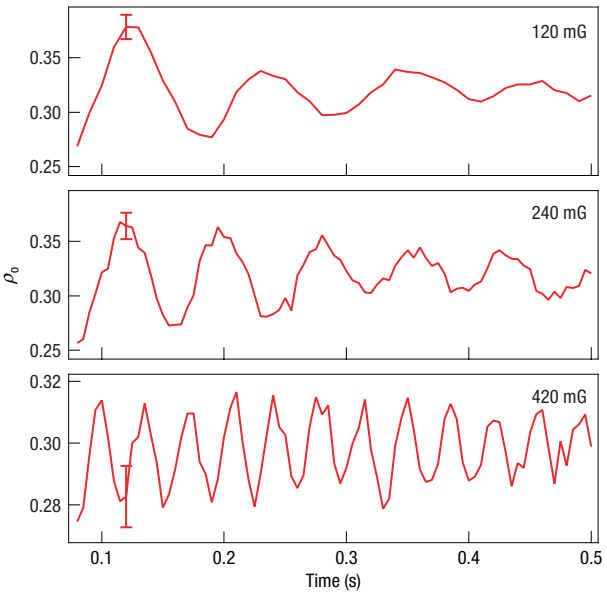

Figure 2 Coherent spin mixing versus magnetic field. An initial non-equilibrium spin-population configuration of $\rho_{(1,0,-1)} \simeq (0, 1/2, 1/2)$ is created and allowed to evolve in a field of 15 mG for 70 ms to allow for maximum spin mixing. At this point, the magnetic field is ramped to different levels. Subsequently, the system shows small-amplitude oscillations analogous to the a.c. Josephson effect, $\rho_0(t) \propto \delta^{-1} \sin 2\delta t$. The typical error bars shown are the standard deviation of three repeated measurements.

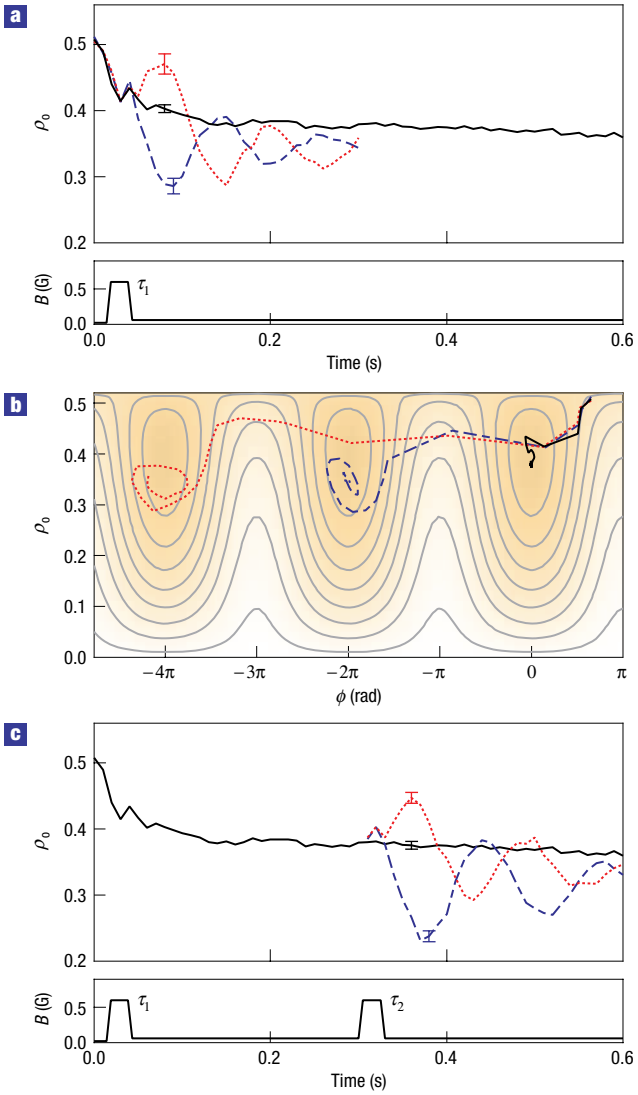

Figure 3 Coherent control of spinor dynamics. a, An initial spin configuration of $\rho_{(1,0,-1)} \simeq (0, 1/2, 1/2)$ is allowed to evolve in a field of 15 mG for 14 ms at which point the populations reach the values corresponding to the ferromagnetic ground state at this magnetization: $\rho_{(1,0,-1)} \simeq (1/16, 3/8, 9/16)$. Then, a pulse of 600 mG field is applied to shift the spinor phase. The dashed, solid and dotted curves represent pulse widths of $\tau_1 = 20, 24.4$ and 30 ms, respectively. For certain applied phase shifts, the coherent spin mixing can be halted. This occurs for $\tau_1 = 24.4$ ms corresponding to the phase shift $\Delta\phi = -2.5\pi$, and for $\tau_1 = 5.3$ ms corresponding to $\Delta\phi = -0.5\pi$. **b**, Reconstructed dynamical trajectories of the system determined by fitting the experiment data to equations (3) and (4) including a phenomenological phase-damping term. The free parameters of the fit are the damping coefficient and the unknown (but reproducible) initial spinor phase resulting from the state preparation, which depends on the applied microwave pulse width and the duration in the upper hyperfine manifold. The contours show curves of equal energy. **c**, To investigate the spin coherence of the ground-state spinor created by the first pulse with $\tau_1 = 24.4$ ms, a second pulse is applied at 300 ms to re-establish the oscillations. The solid, dashed and dotted curves correspond to $\tau_2 = 0, 10$ and 20 ms, respectively. The typical error bars shown are the standard deviation of three repeated measurements.

matches within 10% the prediction $\Omega = 2\delta$, whereas the δ^{-1} scaling for the amplitude is seen only for higher fields, presumably because of the invalidity of the SMA for larger amplitude oscillations. In the future, being able to tune the system to the linear regime provides a path to study many analogous effects previously observed in Josephson systems, such as Shapiro levels[27,36,41,46], by including a time-varying component to the applied magnetic field.

Beyond controlling the system by the initial conditions, the dynamical evolution of the system can be controlled in real time by either changing spin populations and/or changing the spinor phase ϕ. We demonstrate that we can coherently control the dynamical evolution of the spinor by applying phase shifts, and, in particular, we drive the systems to the ferromagnetic spinor ground state using this technique. In this experiment, an initial non-equilibrium spin configuration is created and allowed to evolve for a fraction of an oscillation until $\rho_0(t)$ reaches the ground-state ratio $\rho_{0,\mathrm{gs}} = (1 - M^2)/2$ (refs 23,29). At this point, the system is not in the ground state because $\phi \neq (\phi_{\mathrm{gs}} = 0)$; and it is still oscillating. At this moment, we briefly pulse on a magnetic field of 0.6 G to apply a phase shift to the spinor, $\Delta\phi = \int \delta(t)\,\mathrm{d}t$. The evolution of the system is recorded in Fig. 3a for different pulse durations. We find that, for particular applied phase shifts, the spinor condensate is brought to its ground state, demonstrated by the subsequent lack of population oscillation. For other applied phase shifts, the system is driven to different points in the phase space of the system, for which the subsequent evolution of the system is markedly different and shows oscillations.

It is possible to reconstruct the dynamical trajectories of the system using the measured $\rho_0(t)$, along with the known applied phase shifts and the equations of motion, equations (5) and (6). Although the damping evident in the measurement is owing to the spatial dynamics coupled to the internal spin-mixing dynamics, a phenomenological phase-damping term may be added to equation (6) to represent the spatial varying spin-mixing rate that is responsible for damping the population oscillation. The reconstructed trajectories show good qualitative agreement

with the measurements in the time domain and are plotted on the phase-space diagram of the system (Fig. 3b). Also shown in the figure are the contours of equal energy of the spinor given by equation (4). The trajectories clearly show that the system tends to damp to the minimum energy points (that is, the ferromagnetic spinor ground state), which is $\rho_0 \simeq 3/8, \phi_{gs} = 0 \mod (2\pi)$ for $M = 1/2, c < 0$ and $\delta \approx 0$. For the case of antiferromagnetic interactions, such as in ^{23}Na, $c > 0$, the energy contours differ only in sign, and the system would instead relax to $\rho_0 = 1$, $\phi_{gs} = \pi \mod (2\pi)$ within the validity of the SMA[23,29].

To demonstrate explicitly the coherence of the spinor ground state, we impart a second phase shift to the system at later times to displace the system to a different point in phase space. As anticipated, the second phase shift is found to re-initiate the spin-mixing dynamics (Fig. 3c) when $\Delta\phi \neq 0 \mod (2\pi)$. We have used this technique to determine the ground-state spinor decoherence time by measuring the amplitude of the subsequent oscillations for different delay times of the second pulse. The spinor decoherence time is found to be 3 s, which is approximately the lifetime of the condensate and is much longer than the damping time of spin-population oscillations.

As noted, the damping of the spin oscillations coincides with the appearance of spin wave-like spatial structures in the spinor wavefunction (see the images in Fig. 1b). Hence it is clear that the SMA is not strictly valid for our system. These waves derive their energy from the internal (spin) degrees of freedom, and it is this energy transfer that ultimately damps the spin mixing. On the other hand, if the spinor condensate is driven to its ferromagnetic ground state, as shown in Fig. 3b, there is no internal (spin) energy available for the motional degrees of freedom, and spatial spin structures cannot form. Indeed, in this case, the three spin components are observed to have the same spatial wavefunction and seem to be miscible.

The observation of coherent spinor dynamics in a ferromagnetic spin-1 system reported here paves the way for a host of future explorations. These systems are predicted to manifest complex quantum correlated states showing entanglement and squeezing, and, in general, it will be very interesting to explore the regime of small atom number less than 1,000, where subshot noise effects should become important[21]. Viewing the spin-mixing dynamics as a type of internal-Josephson effect, many future explorations and manipulations of the system can be foreseen following along the path of superconducting weak links. Finally, the coupling of the internal dynamics to the spatial wavefunction can be avoided in future experiments by either decreasing the condensate radii relative to ξ_s and/or operating at high magnetic fields where the timescales for mixing and damping are separated further. In contrast, the coupling of the internal and external degrees of freedom in this system provide a system for exploring nonlinear atom optical phenomena such as spatial–temporal dynamics of four-wave mixing[47].

We note that a group in Mainz, Germany has independently observed coherent spin-mixing oscillations in a Mott state of atoms on a lattice[48]. Their experiment involves a system of many copies of two atoms in each lattice site. In contrast, our system involves a few hundred thousand atoms and the observed coherence reflects the presence of macroscopic quantum fields.

METHODS

To create the condensates, we begin by collecting up to 5×10^8 cold atoms in a simple vapour cell ^{87}Rb magneto-optical trap, which is overlapped with an optical trap formed by a single CO_2 laser beam of 70 W focused to a waist of 60 μm. Up to 3.7×10^7 atoms are loaded into the optical trap, at a density of 4×10^{13} cm^{-3}. To achieve higher densities for efficient evaporation, the trap is compressed immediately after loading by smoothly changing the laser focus to 26 μm over 600 ms using a zoom lens. Simultaneously, the laser power is ramped down over 1.8 s to lower the trap depth and force evaporative cooling. Using this technique, mostly pure condensates containing up to 3×10^5 atoms are created. This technique is not only simple and fast, but also produces condensates ten times larger than in our previous methods[16,19]. The condensates created in this optical trap are generally in a mixture of all $F = 1$ spin states and reveal complicated spatial domains. To create a well-characterized initial condition, we apply a magnetic field gradient during the evaporative cooling[19], which results in pure $m_F = -1$ condensate containing 150,000 atoms—this state is stable against both local and global spin dynamics owing to the conservation of angular momentum. The trap frequencies are $2\pi(190, 170, 17)$ rad s^{-1}, and the condensate density and the Thomas–Fermi radii are estimated to be 2.1×10^{14} cm^{-3} and (3.2, 3.6, 36) μm, respectively. The lifetime of the condensate is measured to be 3 s. Coherent spin state superpositions are created from the pure $m_F = -1$ condensates by applying a sequence of phase-coherent microwave pulses tuned to $F = 1 \leftrightarrow F = 2$ transitions. The pulses are applied at a field of 420 mG to separate out the transitions between the different Zeeman sublevels. Following the pulse sequence, the magnetic field is ramped from 420 to 15 mG in 10 ms. Typical pulse lengths are 20 μs for a $F = 1 \leftrightarrow F = 2$ pulse.

Received 23 June 2005; accepted 3 October 2005; published 30 October 2005.

References

1. Nozières, P. & James, D. S. Particle vs pair condensation in attractive Bose liquids. *J. Phys.* **43,** 1133–1148 (1982).
2. Ensher, J. R., Jin, D. S., Matthews, M. R., Wieman, C. E. & Cornell, E. A. Bose-Einstein condensation in a dilute gas: Measurement of energy and ground-state occupation. *Phys. Rev. Lett.* **77,** 4984–4987 (1996).
3. Burt, E. A. *et al.* Coherence, correlations, and collisions: What one learns about Bose-Einstein condensates from their decay. *Phys. Rev. Lett.* **79,** 337–340 (1997).
4. Andrews, M. R. *et al.* Observation of interference between two Bose condensates. *Science* **275,** 637–641 (1997).
5. Madison, K. W., Chevy, F., Wohlleben, W. & Dalibard, J. Vortex formation in a stirred Bose-Einstein condensate. *Phys. Rev. Lett.* **84,** 806–809 (2000).
6. Matthews, M. R. *et al.* Vortices in a Bose-Einstein condensate. *Phys. Rev. Lett.* **83,** 2498–2501 (1999).
7. Abo-Shaeer, J. R., Raman, C., Vogels, J. M. & Ketterle, W. Observation of vortex lattices in Bose-Einstein condensates. *Science* **292,** 476–479 (2001).
8. Donley, E. A., Claussen, N. R., Thompson, S. T. & Wieman, C. E. Atom-molecule coherence in a Bose-Einstein condensate. *Nature* **417,** 529–533 (2002).
9. Greiner, M., Regal, C. A. & Jin, D. S. Emergence of a molecular Bose-Einstein condensate from a Fermi gas. *Nature* **426,** 537–540 (2003).
10. Greiner, M., Mandel, O., Esslinger, T., Hänsch, T. W. & Bloch, I. Quantum phase transition from a superfluid to a Mott insulator in a gas of ultracold atoms. *Nature* **415,** 39–44 (2002).
11. Anderson, B. P. & Kasevich, M. A. Macroscopic quantum interference from atomic tunnel arrays. *Science* **282,** 1686–1689 (1998).
12. Ho, T. L. Spinor Bose condensates in optical traps. *Phys. Rev. Lett.* **81,** 742–745 (1998).
13. Ohmi, T. & Machida, K. Bose-Einstein condensation with internal degrees of freedom in alkali atom gases. *J. Phys. Soc. Jpn* **67,** 1822–1825 (1998).
14. Hall, D. S., Matthews, M. R., Wieman, C. E. & Cornell, E. A. Measurements of relative phase in two-component Bose-Einstein condensates. *Phys. Rev. Lett.* **81,** 1543–1546 (1998).
15. Stenger, J. *et al.* Spin domains in ground-state Bose-Einstein condensates. *Nature* **396,** 345–348 (1998).
16. Barrett, M. D., Sauer, J. A. & Chapman, M. S. All-optical formation of an atomic Bose-Einstein condensate. *Phys. Rev. Lett.* **87,** 010404 (2001).
17. Gorlitz, A. *et al.* Sodium Bose-Einstein condensates in the $F = 2$ state in a large-volume optical trap. *Phys. Rev. Lett.* **90,** 090401 (2003).
18. Schmaljohann, H. *et al.* Dynamics of $F = 2$ spinor Bose-Einstein condensates. *Phys. Rev. Lett.* **92,** 040402 (2004).
19. Chang, M. S. *et al.* Observation of spinor dynamics in optically trapped Rb-87 Bose-Einstein condensates. *Phys. Rev. Lett.* **92,** 140403 (2004).
20. Koashi, M. & Ueda, M. Exact eigenstates and magnetic response of spin-1 and spin-2 Bose-Einstein condensates. *Phys. Rev. Lett.* **84,** 1066–1069 (2000).
21. Law, C. K., Pu, H. & Bigelow, N. P. Quantum spins mixing in spinor Bose-Einstein condensates. *Phys. Rev. Lett.* **81,** 5257–5261 (1998).
22. Goldstein, E. V. & Meystre, P. Quantum theory of atomic four-wave mixing in Bose-Einstein condensates. *Phys. Rev. A* **59,** 3896–3901 (1999).
23. Pu, H., Law, C. K., Raghavan, S., Eberly, J. H. & Bigelow, N. P. Spin-mixing dynamics of a spinor Bose-Einstein condensate. *Phys. Rev. A* **60,** 1463–1470 (1999).
24. Burke, J. P., Julienne, P. S., Williams, C. J., Band, Y. B. & Trippenbach, M. Four-wave mixing in Bose-Einstein condensate systems with multiple spin states. *Phys. Rev. A* **70,** 033606 (2004).
25. Romano, D. R. & de Passos, E. J. V. Population and phase dynamics of $F = 1$ spinor condensates in an external magnetic field. *Phys. Rev. A* **70,** 043614 (2004).
26. Zhang, W., Zhou, D. L., Chang, M. -S., Chapman, M. S. & You, L. Coherent spin mixing dynamics in a spin-1 atomic condensate. *Phys. Rev. A* **72,** 013602 (2005).
27. Barone, A. & Paterno, G. *Physics and Applications of the Josephson Effect* (Wiley, New York, 1982).
28. Hall, D. S., Matthews, M. R., Ensher, J. R., Wieman, C. E. & Cornell, E. A. Dynamics of component separation in a binary mixture of Bose-Einstein condensates. *Phys. Rev. Lett.* **81,** 1539–1542 (1998).
29. Zhang, W. X., Yi, S. & You, L. Mean field ground state of a spin-1 condensate in a magnetic field. *New J. Phys.* **5,** 77 (2003).
30. Leanhardt, A. E., Shin, Y., Kielpinski, D., Pritchard, D. E. & Ketterle, W. Coreless vortex formation in a spinor Bose-Einstein condensate. *Phys. Rev. Lett.* **90,** 140403 (2003).
31. Kuwamoto, T., Araki, K., Eno, T. & Hirano, T. Magnetic field dependence of the dynamics of Rb-87 spin-2 Bose-Einstein condensates. *Phys. Rev. A* **69,** 063604 (2004).
32. Klausen, N. N., Bohn, J. L. & Greene, C. H. Nature of spinor Bose-Einstein condensates in rubidium. *Phys. Rev. A* **64,** 053602 (2001).

33. van Kempen, E. G. M., Kokkelmans, S. J. J. M. F., Heinzen, D. J. & Verhaar, B. J. Interisotope determination of ultracold rubidium interactions from three high-precision experiments. *Phys. Rev. Lett.* **88,** 093201 (2002).
34. Burke, J. P., Greene, C. H. & Bohn, J. L. Multichannel cold collisions: Simple dependences on energy and magnetic field. *Phys. Rev. Lett.* **81,** 3355–3358 (1998).
35. Duan, L. M., Cirac, J. I. & Zoller, P. Quantum entanglement in spinor Bose-Einstein condensates. *Phys. Rev. A* **65,** 033619 (2002).
36. Pu, H., Raghavan, S. & Bigelow, N. P. Manipulating spinor condensates with magnetic fields: Stochastization, metastability, and dynamical spin localization. *Phys. Rev. A* **61,** 023602 (2000).
37. Miesner, H. J. *et al.* Observation of metastable states in spinor Bose-Einstein condensates. *Phys. Rev. Lett.* **82,** 2228–2231 (1999).
38. Matthews, M. R. *et al.* Watching a superfluid untwist itself: Recurrence of rabi oscillations in a Bose-Einstein condensate. *Phys. Rev. Lett.* **83,** 3358–3361 (1999).
39. Leggett, A. J. Theoretical description of new phases of liquid-He-3. *Rev. Mod. Phys.* **47,** 331–414 (1975).
40. Wheatley, J. C. Experimental properties of superfluid He-3. *Rev. Mod. Phys.* **47,** 415–470 (1975).
41. Davis, J. C. & Packard, R. E. Superfluid ^{3}He weak links. *Rev. Mod. Phys.* **74,** 741–773 (2001).
42. Javanainen, J. Oscillatory exchange of atoms between traps containing Bose condensates. *Phys. Rev. Lett.* **57,** 3164–3166 (1986).
43. Smerzi, A., Fantoni, S., Giovanazzi, S. & Shenoy, S. R. Quantum coherent atomic tunneling between two trapped Bose-Einstein condensates. *Phys. Rev. Lett.* **79,** 4950–4953 (1997).
44. Cataliotti, F. S. *et al.* Josephson junction arrays with Bose-Einstein condensates. *Science* **293,** 843–846 (2001).
45. Cennini, G. *et al.* All-optical realization of an atom laser. *Phys. Rev. Lett.* **91,** 240408 (2003).
46. Shapiro, S. Josephson currents in superconducting tunneling: the effect of microwaves and other observations. *Phys. Rev. Lett.* **11,** 80–82 (1963).
47. Deng, L. *et al.* Four-wave mixing with matter waves. *Nature* **398,** 218–220 (1999).
48. Widera, A. *et al.* Coherent collisional spin dynamics in optical lattices. *Phys. Rev. Lett.* (in the press); preprint at <http://arxiv.org/abs/cond-mat/0505492> (2005).

Acknowledgements

This work was supported by NSF-PHYS 0303013 and NASA-NAG3-2893. We would like to thank C. D. Hamley, K. M. Fortier, J. A. Sauer and other members of the Georgia Tech Atomic Physics and Quantum Optics Group for their assistance, and H. Pu for valuable discussions.
Correspondence and requests for materials should be addressed to M.S.C.

Competing financial interests

The authors declare that they have no competing financial interests.